Using Otoacoustic Emissions to Measure the Transmission Matrix of the Middle-ear

by

Antonio John Miller

B.S., Mathematical and Computer Sciences, Colorado School of Mines (1997)
M.S., Acoustics, Pennsylvania State University (1999)

Submitted to the Harvard-MIT Division of Health Sciences and Technology
in partial fulfillment of the requirements for the degree of

Master of Science in Health Sciences and Technology

at the

MASSACHUSETTS INSTITUTE OF TECHNOLOGY

September 2006

Author .....
Harvard-MIT Division of Health Sciences and Technology
August 31, 2006

Certified by .....
Christopher A. Shera, Ph.D.
Assoc. Prof. of Otology and Laryngology, Harvard Medical School
Thesis Supervisor

Accepted by .....
Martha Gray, Ph.D.
Edwin Hood Taplin Professor of Medical and Electrical Engineering
Co-director, Harvard-MIT Division of Health Sciences and Technology

Using Otoacoustic Emissions to Measure the Transmission Matrix of the Middle-ear

by

Antonio John Miller

Submitted to the Harvard-MIT Division of Health Sciences and Technology
on August 30, 2006, in partial fulfillment of the
requirements for the degree of
Master of Science in Health Sciences and Technology

Abstract

Here we describe an experimental method for measuring the acoustic transmission matrix of the middle-ear using otoacoustic emissions. The experiment builds on previous work that uses distortion product otoacoustic emissions (DPOAEs) as an intracochlear sound source to drive the middle-ear in reverse. This technique eliminates the complications introduced by needing to place an acoustic transducer inside the cochlea. Previous authors have shown how the complete 4x3 system response matrix, with its 12 unknowns, can be simplifed to a 2x2 transmission matrix by decoupling the middle-ear cavity and assuming the cochlear fluids are incompressible. This simplified description of middle-ear mechanics assumes that the input-output response at the tympanic membrane and stapes footplate is linear, one dimensional and time invariant. The technique allows for estimating the acoustic pressure and volume velocity at the tympanic membrane and the volume velocity of the stapes footplate, in both the forward and reverse direction, and under different boundary conditions at the stapes. The technique was applied to deeply anesthetized cats with widely opened middle-ear cavities over a frequency range of 200Hz to 10kHz. Results on three animals are reported and generally agree with previous data and a published middle-ear model.

Thesis Supervisor: Christopher A. Shera, Ph.D.
Title: Assoc. Prof. of Otology and Laryngology, Harvard Medical School

Little by little, hearing became my favorite sense; for just as it is the voice that reveals the inwardness which is incommensurable with the outer, so the ear is the instrument whereby that inwardness is grasped, hearing the sense by which it is appropriated.

-Søren Kierkegaard

Contents

List of Figures

Chapter 1

Introduction

1.1 Middle-ear Anatomy

The peripheral auditory system is composed of three major components – the external ear, the middle-ear and the inner-ear. Figure 1-1 illustrates the basic anatomy of the middle-ear, using a coronal section of the human head. Briefly, the tympanic membrane terminates the end of the earcanal and is attached to the malleus, the first of the three middle-ear bones. The malleus forms a joint with the incus, which in turn, forms the incudo-stapedial joint with the stapes. The stapes footplate is then attached via the annular ligament to the oval window of the cochlea.

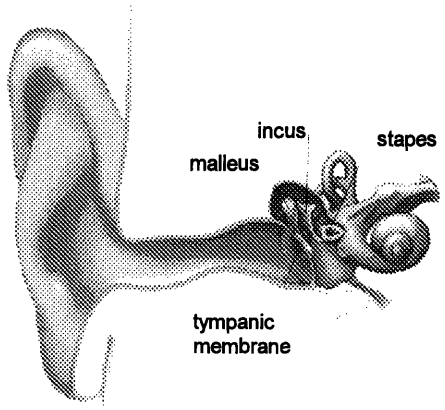

Figure 1-1: Basic Anatomy of the Human Middle-ear [11].

1.2 Middle-ear Physiology

The mammalian middle-ear is a real marvel of acoustic design. Its function has evolved to help bridge the three orders of magnitude difference in characteristic acoustic impedance between the air of the surrounding environment and the cochlear fluids that are vital to normal transduction of sound in the inner-ear. Consider Figure 1-2 as a simple example of what the middle-ear has to overcome.

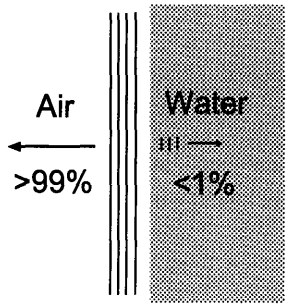

Figure 1-2: Acoustic Power Reflected from an Air/Water Interface.

An acoustic plane wave incident at an air/water interface undergoes almost complete reflection – equation 1.1 shows that less than 1 percent of the power is transmitted to the liquid. In the absence of a middle-ear, this impedance mismatch would greatly impair an animal's ability to detect sound.

$$\|\mathcal{R}\|^2 = \left\| \frac{\left(\frac{Z_{\text{water}}}{Z_{\text{air}}} - 1\right)}{\left(\frac{Z_{\text{water}}}{Z_{\text{air}}} + 1\right)} \right\|^2 > 0.99 \tag{1.1}$$

In the clinic, middle-ear disorders comprise the majority of audiological visits and are often successfully treated through medication, surgery or amplification when properly diagnosed. The noninvasive assessment of middle-ear function remains a major challenge and the use of otoacoustic emissions may allow for improved diagnostic methods.

1.3 Distortion Product Otoacoustic Emissions

While the importance of the forward transmission of sound through the middle-ear has been explored for some time, the reverse transmission has only recently been receiving greater attention. This is largely due to the need to quanitatively understand how otoacoustic emissions can be used as noninvasive probes of auditory function. Most normal hearing people have measurable sound that is emitted from their ears, both spontaneously and under an evoking stimulus. When the evoking stimulus is two tones, say f_1 and f_2, the largest of the resulting nonlinear distortion products (DPOAEs) is $2f_1 - f_2$. The DPOAE has been shown to be generated inside the cochlea via several mechanisms [15] where it then propagates back through the middle-ear. The reverse propagation of the DPOAE, as depicted schematically in Figure 1-3, is what will allow us to measure the reverse transmission of sound through the middle-ear.

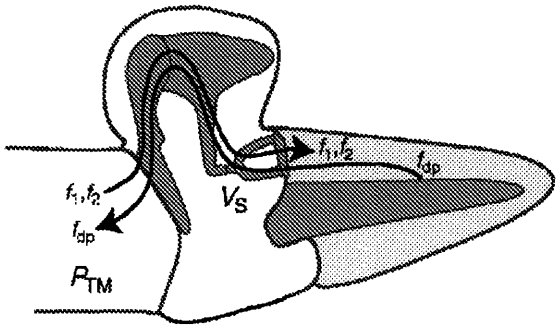

Figure 1-3: Schematic of the Propagation of DPOAEs from Ref [18].

1.4 Acoustic Transmission Matrix

The transmission (or ABCD) matrix is a useful way of quantifying the complete input-output response of an acoustic transducer. By finding the matrix elements, we are able to mathematically isolate the system response from any loading at the terminals. Equation 1.2 is the basic statement of the acoustic transmission matrix.

$$\begin{pmatrix} P_{in} \\ U_{in} \end{pmatrix} = \begin{pmatrix} A & B \\ C & D \end{pmatrix} \begin{pmatrix} P_{out} \\ U_{out} \end{pmatrix} \tag{1.2}$$

The input power vector equals the transmission matrix times the output power vector. We are able to solve for the matrix elements by setting each of the outputs equal to zero and solving for the remaining variables as seen in matrix equation 1.3.

$$\begin{pmatrix} A & B \\ C & D \end{pmatrix} = \begin{pmatrix} \frac{P_{\text{in}}}{P_{out}}\Big|_{U_{out}=0} & \frac{P_{\text{in}}}{U_{out}}\Big|_{P_{out}=0} \\ \frac{U_{\text{in}}}{P_{out}}\Big|_{U_{out}=0} & \frac{U_{\text{in}}}{U_{out}}\Big|_{P_{out}=0} \end{pmatrix} \tag{1.3}$$

Solving for the matrix elements allows us to quantify the system performance of the middle-ear independent of the impedances presented by the earcanal source or the cochlear input impedance. This approach also allows us to directly compare theory and experiment by relating middle-ear model parameters directly to measureable quantities.

Figure 1-4 illustrates how we can conceptualize the middle-ear as a 2-port transmission matrix. The input to the system is an acoustic plane wave in front of the tympanic membrane, while the output is the one dimensional fluid motion of the stapes footplate. Previous authors [18] have argued that there is considerable experimental evidence to justify both the assumption of one dimensional motion and the system's linearity. The remaining assumption that the system remains time-invariant is largely a function of the experimenter's skill at keeping the middle-ear in good working condition during the course of an experiment.

We can then define matrix equation 1.4 in terms of the input pressure P_{tm} and volume velocity U_{tm} at the tympanic membrane, the middle-ear transmission matrix elements (A_{me}, B_{me}, C_{me}, D_{me}) and the output pressure P_{st} and volume velocity U_{tm} at the stapes.

$$\begin{pmatrix} P_{tm} \\ U_{tm} \end{pmatrix} = \begin{pmatrix} A_{me} & B_{me} \\ C_{me} & D_{me} \end{pmatrix} \begin{pmatrix} P_{st} \\ U_{st} \end{pmatrix} \tag{1.4}$$

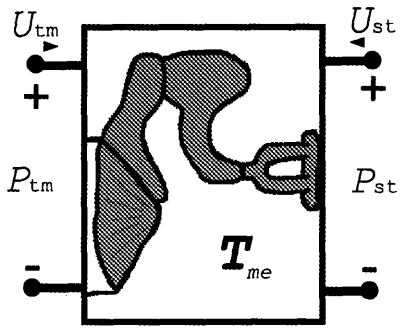

Figure 1-4: Schematic of the Middle-ear as an Acoustic 2-Port Transmission Matrix.

1.5 Solving the System Equations

Our experimental paradigm is able to measure three variables (P_{tm}, U_{tm}, U_{st}), the remaining variables are unknown, and are shown in bold in equation 1.5. In total, there are five unknowns ($\boldsymbol{A_{me}}$, $\boldsymbol{B_{me}}$, $\boldsymbol{C_{me}}$, $\boldsymbol{D_{me}}$, $\boldsymbol{P_{st}}$) shown in bold in matrix equation 1.5.

$$\begin{pmatrix} P_{\mathrm{tm}} \\ U_{\mathrm{tm}} \end{pmatrix} = \begin{pmatrix} \boldsymbol{A_{me}} & \boldsymbol{B_{me}} \\ \boldsymbol{C_{me}} & \boldsymbol{D_{me}} \end{pmatrix} \begin{pmatrix} \boldsymbol{P_{st}} \\ U_{st} \end{pmatrix} \tag{1.5}$$

Solving for the unknowns requires us to find five algebraic equations that relate the measurement variables to the unknowns. The intact middle-ear driven in the forward direction, produces the two equations that are shown below. Where superscript 'int' simply refers to the measurement variable in the intact case.

$$\overset{\mathrm{int}}{P}_{\mathrm{tm}} = \boldsymbol{A_{me}}\overset{\mathbf{int}}{\boldsymbol{P}}_{\mathbf{st}} + \boldsymbol{B_{me}}\overset{\mathrm{int}}{U}_{\mathrm{st}} \tag{1.6}$$

$$\overset{\mathrm{int}}{U}_{\mathrm{tm}} = \boldsymbol{C_{me}}\overset{\mathbf{int}}{\boldsymbol{P}}_{\mathbf{st}} + \boldsymbol{D_{me}}\overset{\mathrm{int}}{U}_{\mathrm{st}} \tag{1.7}$$

Draining the cochlea imposes an acoustic 'open-circuit' at the stapes. This condition allows us to solve the following two equations. The superscript 'drn' refers to the drained cochlea.

$$\boldsymbol{B_{me}} = \frac{\overset{\text{drn}}{P_{\text{tm}}}}{\underset{\text{drn}}{U_{\text{st}}}} \tag{1.8}$$

$$\boldsymbol{D_{me}} = \frac{\overset{\text{drn}}{U_{\text{tm}}}}{\underset{\text{drn}}{U_{\text{st}}}} \tag{1.9}$$

For the fifth equation, we have a choice of three different equations. We can choose to use an equation for the reverse transfer function 1.10, an equation for middle-ear reciprocity, or an equation for the input impedance when the stapes footplate is fixed. In the results section we have shown the transmission matrix results using both the reverse transfer function and middle-ear reciprocity. The discussion section suggests incorporating the stapes fixation case into future experiments.

$$T_{rev} = \frac{A_{st} Z_{\text{src}}}{\boldsymbol{A_{me}} + \boldsymbol{C_{me}} Z_{\text{src}}} \tag{1.10}$$

Using the reverse transfer function 1.10, we arrive at the following solutions -1.14 for the matrix elements.

$$\boldsymbol{A_{me}} = \frac{\left(\overset{\text{int drn}}{P_{\text{tm}} U_{\text{st}}} - \overset{\text{drn int}}{P_{\text{tm}} U_{\text{st}}} \right) A_s Z_{\text{src}}}{T_{rev} \left(\overset{\text{int drn}}{P_{\text{tm}} U_{\text{st}}} - \overset{\text{drn int}}{P_{\text{tm}} U_{\text{st}}} + \left(\overset{\text{int drn}}{-U_{\text{st}} U_{\text{tm}}} + \overset{\text{drn int}}{U_{\text{st}} U_{\text{tm}}} \right) Z_{\text{src}} \right)} \tag{1.11}$$

$$\boldsymbol{B_{me}} = \frac{\overset{\text{drn}}{P_{\text{tm}}}}{\underset{\text{drn}}{U_{\text{st}}}} \tag{1.12}$$

$$\boldsymbol{C_{me}} = \frac{\left(\overset{\text{int drn}}{U_{\text{st}} U_{\text{tm}}} - \overset{\text{drn int}}{U_{\text{st}} U_{\text{tm}}} \right) A_s Z_{\text{src}}}{T_{rev} \left(\overset{\text{int drn}}{-P_{\text{tm}} U_{\text{st}}} + \overset{\text{drn int}}{P_{\text{tm}} U_{\text{st}}} + \left(\overset{\text{int drn}}{U_{\text{st}} U_{\text{tm}}} - \overset{\text{drn int}}{U_{\text{st}} U_{\text{tm}}} \right) Z_{\text{src}} \right)} \tag{1.13}$$

$$\boldsymbol{D_{me}} = \frac{\overset{\text{drn}}{U_{\text{tm}}}}{\underset{\text{drn}}{U_{\text{st}}}} \tag{1.14}$$

Whereas, using the reciprocity condition 1.15, we arrive at a somewhat simplier set of solutions 1.16-1.19 for the matrix elements.

$$\boldsymbol{A_{me}D_{me}} - \boldsymbol{B_{me}C_{me}} = 1 \tag{1.15}$$

$$\boldsymbol{A_{me}} = \frac{\overset{\text{int}}{P_{\text{tm}}}\overset{\text{drn}}{U_{\text{st}}} - \overset{\text{drn}}{P_{\text{tm}}}\overset{\text{int}}{U_{\text{st}}}}{\overset{\text{int}}{P_{\text{tm}}}\overset{\text{drn}}{U_{\text{tm}}} - \overset{\text{drn}}{P_{\text{tm}}}\overset{\text{int}}{U_{\text{tm}}}} \tag{1.16}$$

$$\boldsymbol{B_{me}} = \frac{\overset{\text{drn}}{P_{\text{tm}}}}{\overset{\text{drn}}{U_{\text{st}}}} \tag{1.17}$$

$$\boldsymbol{C_{me}} = \frac{\overset{\text{int}}{U_{\text{st}}}\overset{\text{drn}}{U_{\text{tm}}} - \overset{\text{drn}}{U_{\text{st}}}\overset{\text{int}}{U_{\text{tm}}}}{-\overset{\text{int}}{P_{\text{tm}}}\overset{\text{drn}}{U_{\text{tm}}} + \overset{\text{drn}}{P_{\text{tm}}}\overset{\text{int}}{U_{\text{tm}}}} \tag{1.18}$$

$$\boldsymbol{D_{me}} = \frac{\overset{\text{drn}}{U_{\text{tm}}}}{\overset{\text{drn}}{U_{\text{st}}}} \tag{1.19}$$

As a sidenote, future experiments could include an additional equation for stapes fixation 1.20.

$$\frac{\overset{\text{fix}}{P_{\text{tm}}}}{\overset{\text{fix}}{U_{\text{tm}}}} = \frac{\boldsymbol{A_{me}}}{\boldsymbol{C_{me}}} \tag{1.20}$$

Chapter 2

Methods

2.1 Overview

The measurements were performed on five anesthetized cats in a sound isolation chamber in the Eaton-Peabody Laboratory at the Massachusetts Eye and Ear Infirmary. The measurement system consisted of a PC running the Microsoft Windows XP operating system and custom MATLAB software that communicates with a Tucker-Davis Technologies RP2.1 signal processor. Signals were created in MATLAB and downloaded to memory buffers on the signal processor. The RP2.1 ran a real time signal averaging algorithm and kept the averaged responses in memory. When the signal averaging was complete, the result was downloaded, displayed and stored on the PC hard drive. The acoustic assembly consisted of an Etymotic Research ER-10C microphone and two ER-3 sound sources. A commerical Polytek OFV-501 laser vibrometer was used to measure stapes velocity and the carrier signal strength was monitored via audio feedback using custom built electronics to demodulate the carrier signal strength. A block diagram of the experimental setup is shown in figure 2-1.

2.2 Animal Preparation

Measurements were made on one (or both) ears of deeply anesthetized cats in a sound isolation chamber at the Eaton-Peabody Laboratory. Animals were treated according

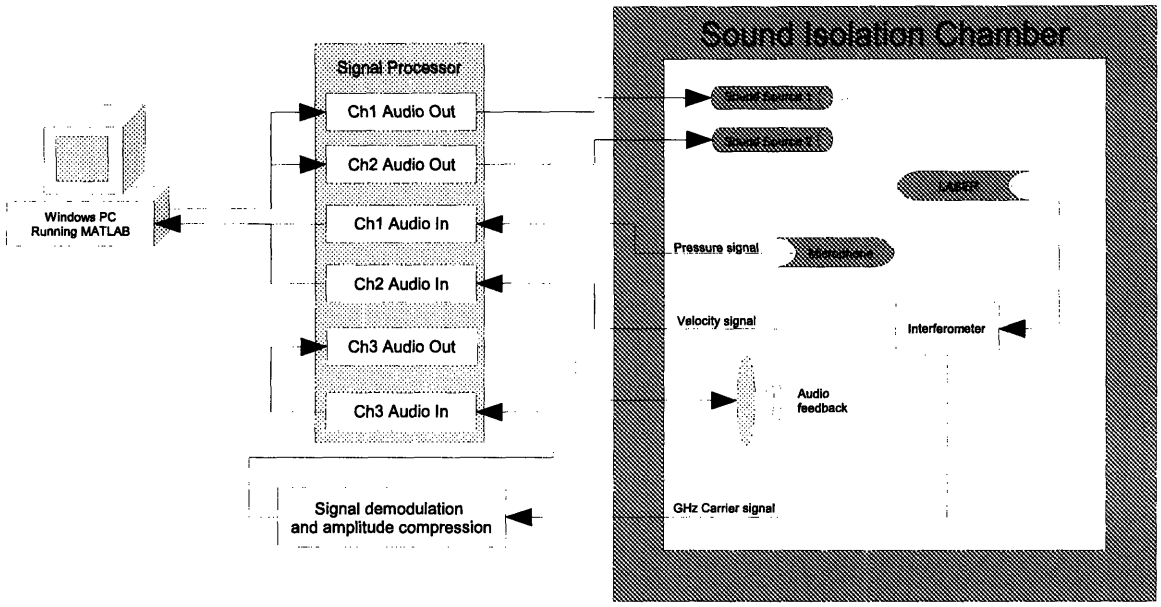

Figure 2-1: Block Diagram of the Experimental Setup.

to approved protocols of the animal care committee at the Massachusetts Eye and Ear Infirmary. Five cats with a median age of 111 days and weighing between 1.7 and 2.5 kilograms were anesthetized using IP injections of Dial at 75mg/kg. Ten percent of the initial dose was given as a booster during the course of the experiment in response to withdrawl from toe pinch. Animal body temperature was continously monitored and the sound isolation chamber was humidified to prevent the middle-ear from drying. The surgical technician removed the pinna and most of the cartilaginous ear canal to allow the acoustic assembly to be placed within 3 to 5mm of the tympanic membrane. The bulla's ventral and lateral walls were removed along with most of the bony septum. Figure 2-3 illustrates how the temporal bone was drilled to gain visual assess to the incudo-stapedial joint. A small piece of reflective tape was adhered to the joint by hand under magnification, and the laser was manually aligned using a micromanipulator and a audio feedback signal to determine if the laser was hitting the target.

2.3 Measurement System and Stimulus Generation

Ear-canal pressure P_{ec} was generated and measured with calibrated transducers positioned within 3-5 mm of the tympanic membrane. Signals were generated, recorded and displayed using MATLAB. The earphones were Etymotic Research model ER-3, which were modified to include additional acoustic damping material to help prevent the high output sound sources from interacting during the measurement of DPOAEs. The low noise microphone was from an Etymotic Research ER-10C assembly. The ER-10C preamplifier was used to amplify the signals 40dB. Two different types of stimuli were used – a broadband chirp signal and a two tone complex. The chirp signals were used to quickly measure the input impedance and forward transfer function. The two tone complex was used to measure the DPOAEs emitted from the cochlea. The DPOAE primary tone frequency ratio f_1/f_2 was held fixed at 1.2 and the level difference $L_1 - L_2$ was held at 5 dBSPL. Response magnitude and angle were obtained from the 4096-point FFT of the time-domain average of a large number of responses sampled at 48.828 kHz. Typically DPOAEs were measured using 1024 averages, whereas, 128 averages were used to measure the chirp reponses.

2.4 Measurement of Stapes Velocity

Visual access to the stapes was obtained by drilling the temporal bone at McEwens triangle using a variable speed dental drill. Care was taken to minimize bleeding or any damage to the delicate middle-ear ossicles. A small piece of reflective tape was placed on the incudo-stapedial joint using the aid of microscope magnification. The Doppler-shifted reflected signal was detected and decoded in hardware by the vibrometer to produce an output voltage that was proportional to stapes velocity. The vibrometer output voltage was amplified by a factor of 10 or 100 depending upon the amount of voltage headroom available. Previous authors [18] have shown that placing the reflective target does not alter ossicular motion.

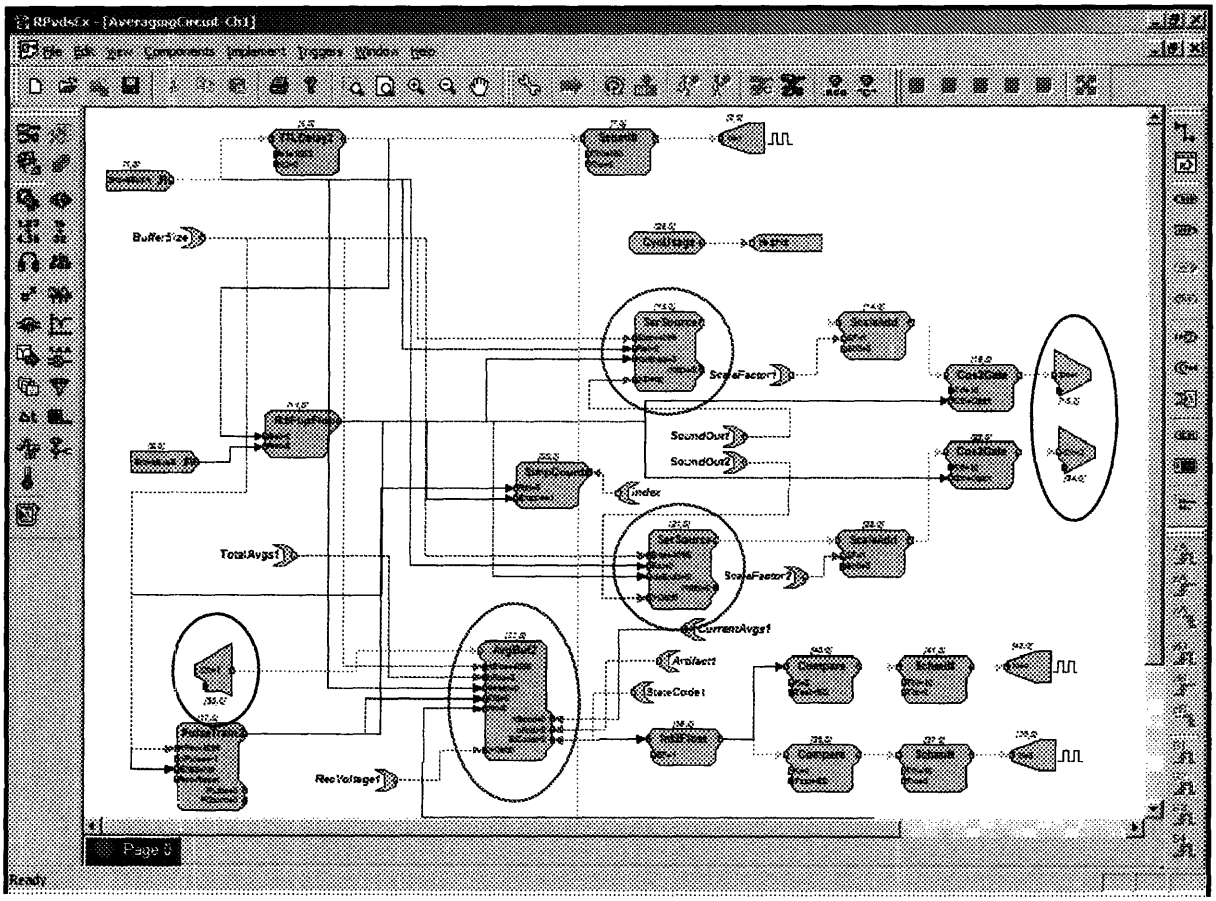

Figure 2-2: Tucker-Davis Technologies Real-Time Signal Processing Circuit Schematic. Input, Outputs and Signal Buffers are Circled.

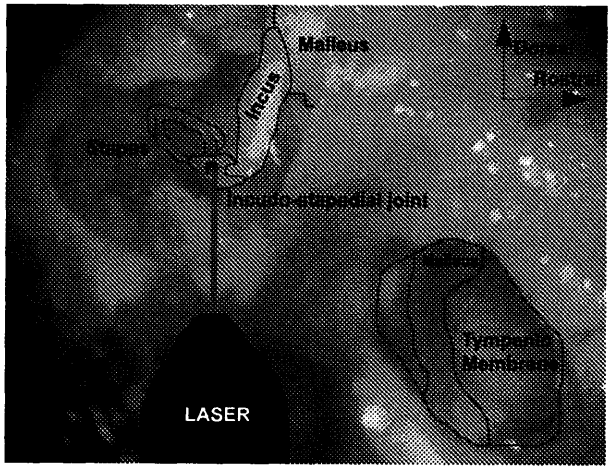

Figure 2-3: View of the stapes exposure in relation to the earcanal.

2.4.1 Stapes Velocity Noisefloor

The most time intensive part of the experiment was being able to measure the DPOAE in the stapes velocity signal. Experience taught us that a very large number of signal averages were required to pull the distortion product signal out of the stapes velocity noise floor. Since we did not know beforehand how many averages were required to meet a specified signal to noise ratio (SNR), we implemented an algorithium in MATLAB that continously computed the SNR of the DPOAE. The stapes velocity noise floor was calculated from the average of the six sound pressure levels of the frequency bins surrounding the distortion product frequency. The software then continously checked to see whether the minimum SNR condition was met, or if the maximum number of averages had been reached. If either condition was satisifed, the software would signal the end of that measurement frequency and begin the next frequency. This approach allowed us to save a considerable amount of time when we had either a strong velocity signal or a large DPOAE.

2.5 Acoustic Impedance Measurements

In order to measure acoustic impedance, the Etymotic Research ER-10C acoustic assembly is first calibrated using the a reference calibration technique. A 1/4" Bruel & Kjaer reference microphone was placed in a Larson-Davis 250Hz tone calibrator to obtain the microphone sensitivity. The reference microphone is then assumed to obey its factory calibration and have a flat frequency response over the audible frequency range of 20Hz to 20kHz (+/-1dB). The reference microphone is then coupled to the ER-10C using a small cylinderical cavity with a diameter approximating the cat ear canal. A broadband chirp is played from one of the ER-3 sound sources and the resulting averaged frequency response is measured using both the reference microphone and the ER-10C microphone. Since the cavity volume is very small, we can assume the two microphones are measuring the same sound field. This assumption allows us to equate the two responses and derive a linear voltage to pressure frequency response for the ER-10C microphone assembly.

The impedance calibration of the acoustic assembly is then accomplished by finding the equivalent Thevenin source impedance and pressure using a least squares error approach as described in Voss and Allen [16]. The pressure response of four brass tubes with known diameter, length and temperature are measured. Using a simple acoustic pressure divider circuit with equivalent source pressure P_{src} and impedance Z_{src}, each of the tube's pressure reponses are measured $P_{i=1,2,3,4}$. A transmission line acoustic impedance model [4] for each tube $Z_{i=1,2,3,4}$ is then used to form the following matrix equation 2.1.

$$\begin{pmatrix} Z_1 & -P_1 \\ Z_2 & -P_2 \\ Z_3 & -P_3 \\ Z_4 & -P_4 \end{pmatrix} \begin{pmatrix} P_{\text{src}} \\ Z_{\text{src}} \end{pmatrix} = \begin{pmatrix} Z_1 P_1 \\ Z_2 P_2 \\ Z_3 P_3 \\ Z_4 P_4 \end{pmatrix} \tag{2.1}$$

The lossy transmission line impedance model for cylinderical cavity impedances [4] has one free parameter – the tube length. Initial guesses for the tube lengths are calculated from the first zero in the pressure response. This notch frequency is the quarter wavelength resonance, which combined with an accurate estimate of the sound speed, give a good initial estimate of the tube length. The initial guesses for all four tube lengths are input to the MATLAB optimization tool fminsearch' which searches the error space for the four length combinations which minimize the mean square error. Once MATLAB has converged on an optimal solution, the resulting source pressure and impedance are verified by measuring an additional set of four tubes of differing lengths. The source pressure and impedance are then used to calculate the acoustic impedance of the second set of tubes. The resulting acoustic impedances are compared to the lossy model to verify the ability of this set of source parameters to accurately measure unknown impedances. Figure 2-4 shows an example for the calculated source pressure and impedance for the ER-10C assembly.

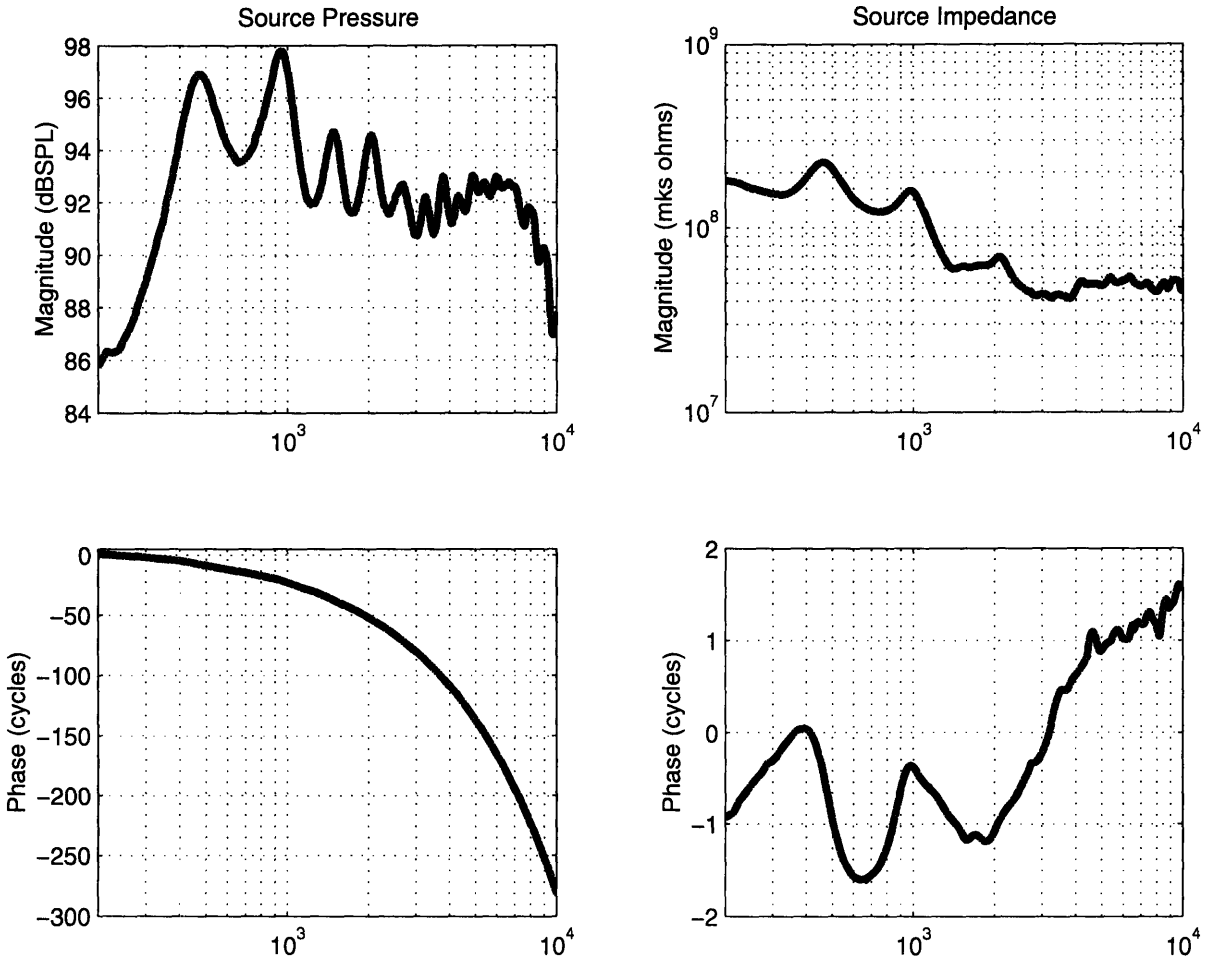

Figure 2-4: Thevenin Equivalent Source Parameters for the Acoustic Probe Assembly.

2.5.1 Residual Earcanal Space

Since we are measuring the acoustic pressure a small distance from the tympanic membrane, we need to make a correction to the ear canal pressure measurements to account for the additional volume of the ear canal. Several authors have previously dealt with this question [1, 6, 9, 19]. Briefly, the method is to describe the space between the measurement system and the tympanic membrane as a circular tube, of cross sectional area A and length l. This approach allows us to define the transmission matrix 2.2 that transforms the ear canal pressure P_{ec} and volume velocity U_{ec} to its equivalent pressure P_{tm} and volume velocity P_{tm} at the tympanic membrane using the transmission line characteristic impedance $Z_o = \frac{\rho c}{A}$.

$$\begin{pmatrix} P_{\mathrm{ec}} \\ U_{\mathrm{ec}} \end{pmatrix} = \begin{pmatrix} \cosh(ikl) & Z_0 \cdot \sinh(ikl) \\ \frac{1}{Z_0} \cdot \sinh(ikl) & \cosh(ikl) \end{pmatrix} \begin{pmatrix} P_{\mathrm{tm}} \\ U_{\mathrm{tm}} \end{pmatrix} \tag{2.2}$$

2.6 Stability of the Preparation

Several steps were taken during the experiment to assure that the transmission properties of the middle-ear remained unchanged. The experimental chamber was equiped with a humidifer to help keep the middle-ear from drying out. The animal's temperature was maintained by heating the chamber and using an electric heating blanket. Additionally, sterile saline was used to periodically moisten the middle-ear. Shortening the length of time required to get a complete set of measurements helps to ensure the stability of the preparation over the course of the experiment.

Chapter 3

Results

3.1 Transfer Functions

The in-the-ear calibration uses a broadband chirp response which can also be used for the measurement of the forward transfer function. It is important to verify that the broadband response is equivalent to measuring the forward transfer function using tones. Figure 3-1 shows the forward transfer function for Cat005 using 3 different DPOAE sweep measurements and the result using the broadband chirp. The two advantages of the broadband chirp response is the speed with which it is measured - it is acquired in the same time as it takes to measure just one DPOAE frequency point and the fact that it covers the entire frequency domain of interest. Since both methods appear to be measuring the same forward transfer function, the broadband chirp method is preferred.

3.1.1 Forward and Reverse Transfer Functions

In the following series of plots, the tympanic membrane pressure P_{tm} is plotted as a function of frequency in the first panel, the stapes velocity v_{st} is in the second panel, and the transfer functions are in the third panel. The very highest curves are the primary tones, the middle curves are the DPOAE levels, and the bottom points are the noise floor estimates (see Figures 3-2, 3-3 and 3-4).

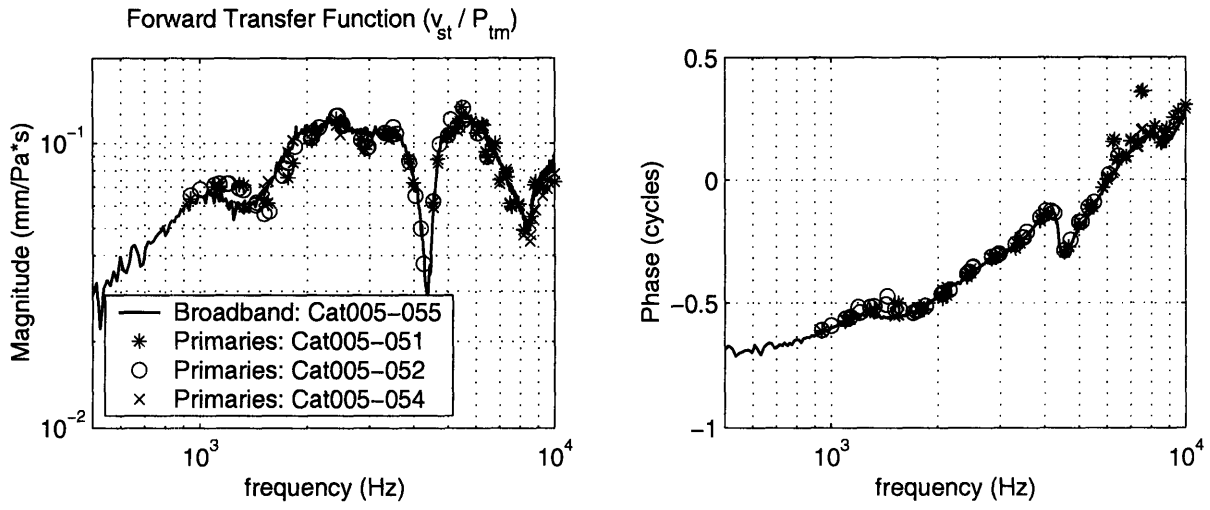

Figure 3-1: Forward Transfer Functions Measured Using Broadband Chirp and DPOAE Primary Tones.

3.2 Acoustic Impedance Measurements

Figure 3-5 is a plot of a typical input impedance at the tympanic membrane overlayed with the Thevenin source impedance. We can note that there will be problems estimating the acoustic impedance for low frequencies, since the input impedance is no longer small compared to the source impedance.

3.3 Transmission Matrix Elements

Here we show the calculation of the transmission matrix elements for Cat005 (Figure 3-6 and 3-7). Included in the graphs are representative data from the Voss and Shera paper [19] and Puria and Allen model results [7]. Note the large deviations of the measurements at low frequencies, especially in the phase plots. This deviation may be linked to poor estimates of the tympanic membrane volume velocity at low frequencies.

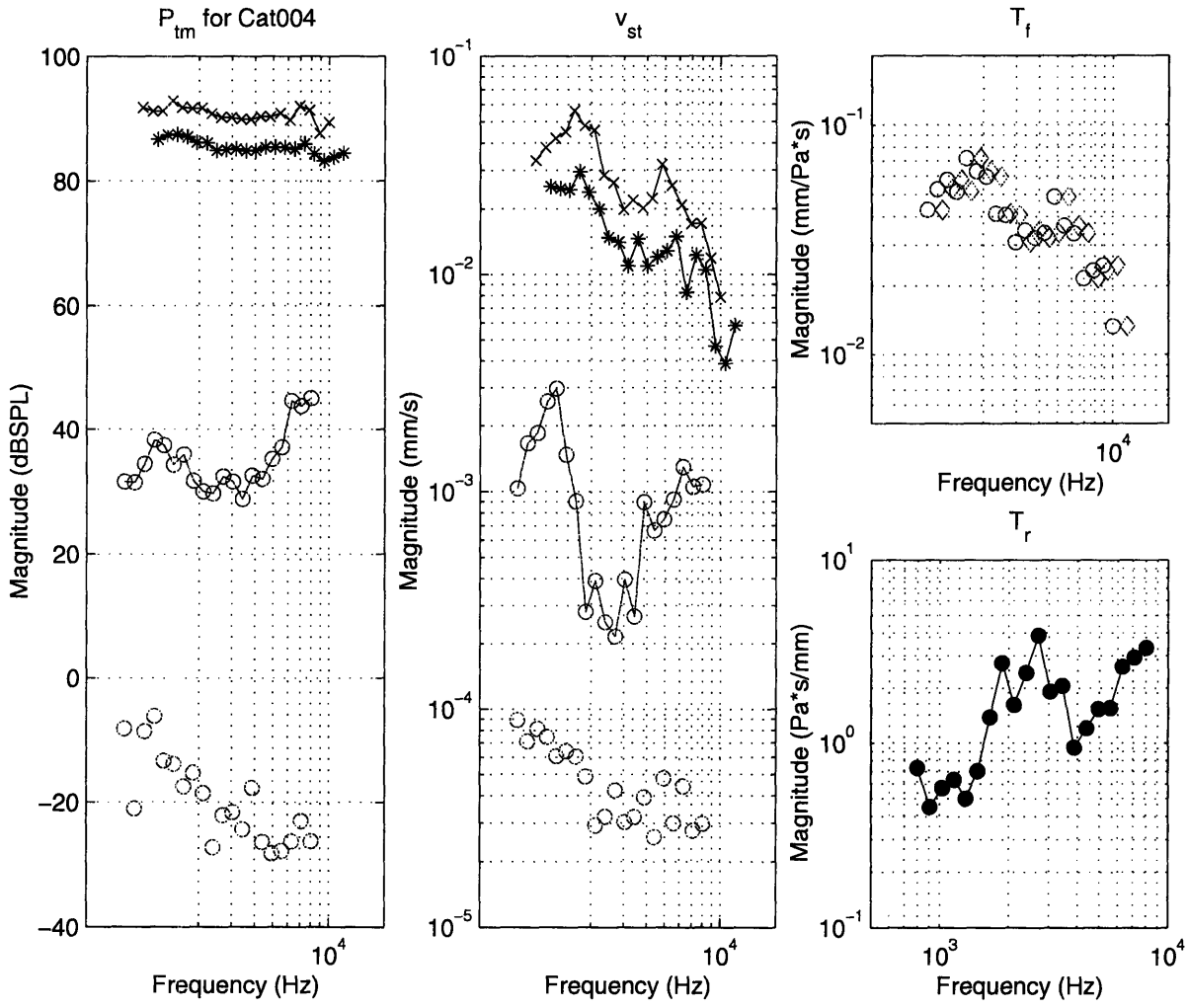

Figure 3-2: Measurements of earcanal pressure and stapes velocity using DPOAEs for Cat004.

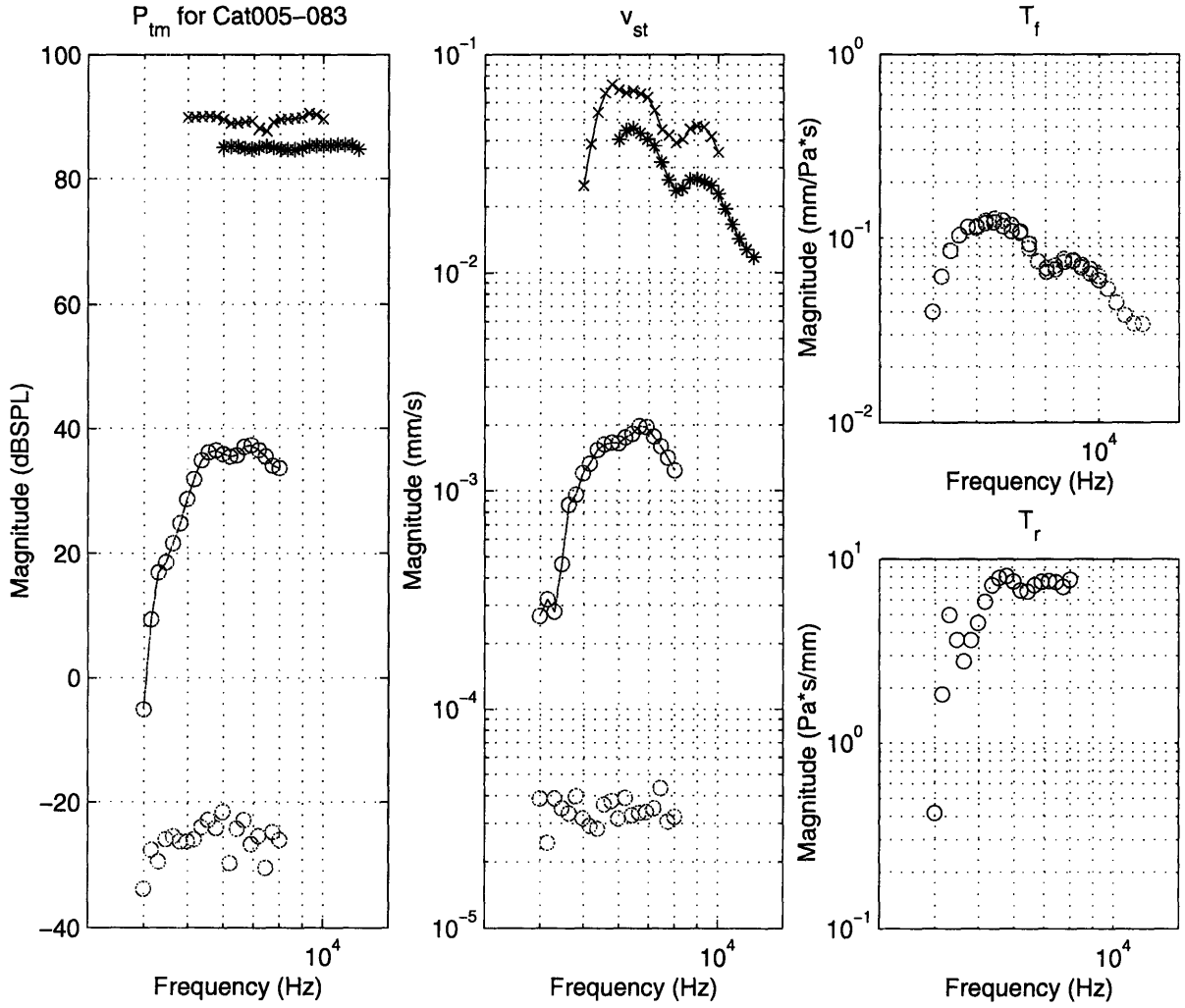

Figure 3-3: Measurements of earcanal pressure and stapes velocity using DPOAEs for Cat005.

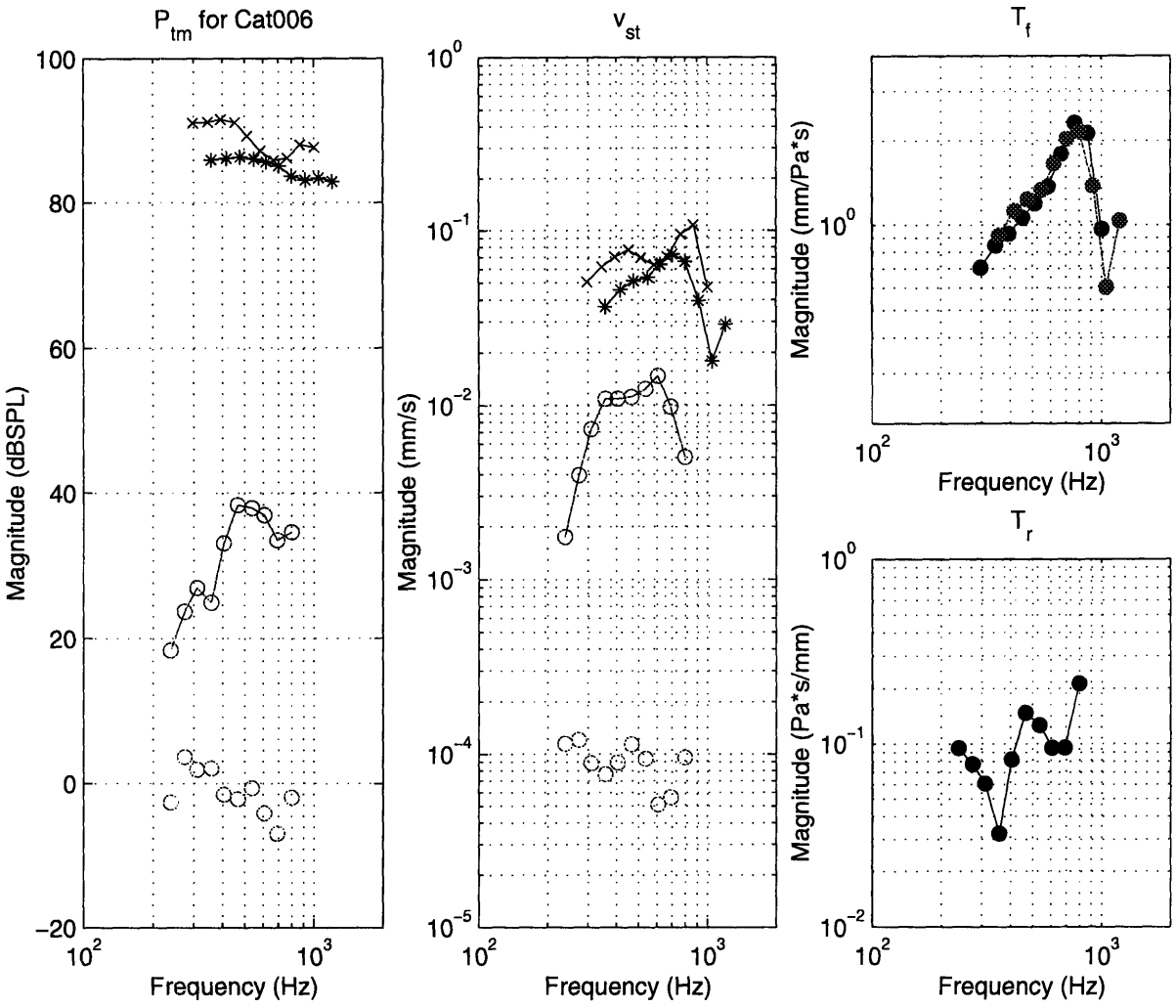

Figure 3-4: Measurements of earcanal pressure and stapes velocity using DPOAEs for Cat006.

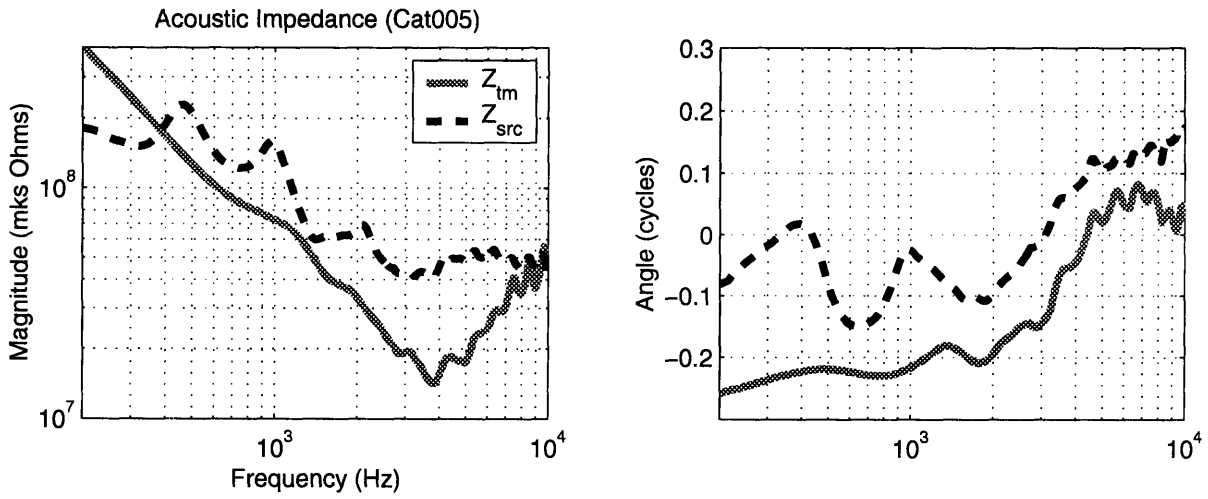

Figure 3-5: Acoustic Impedance at the Tympanic Membrane.

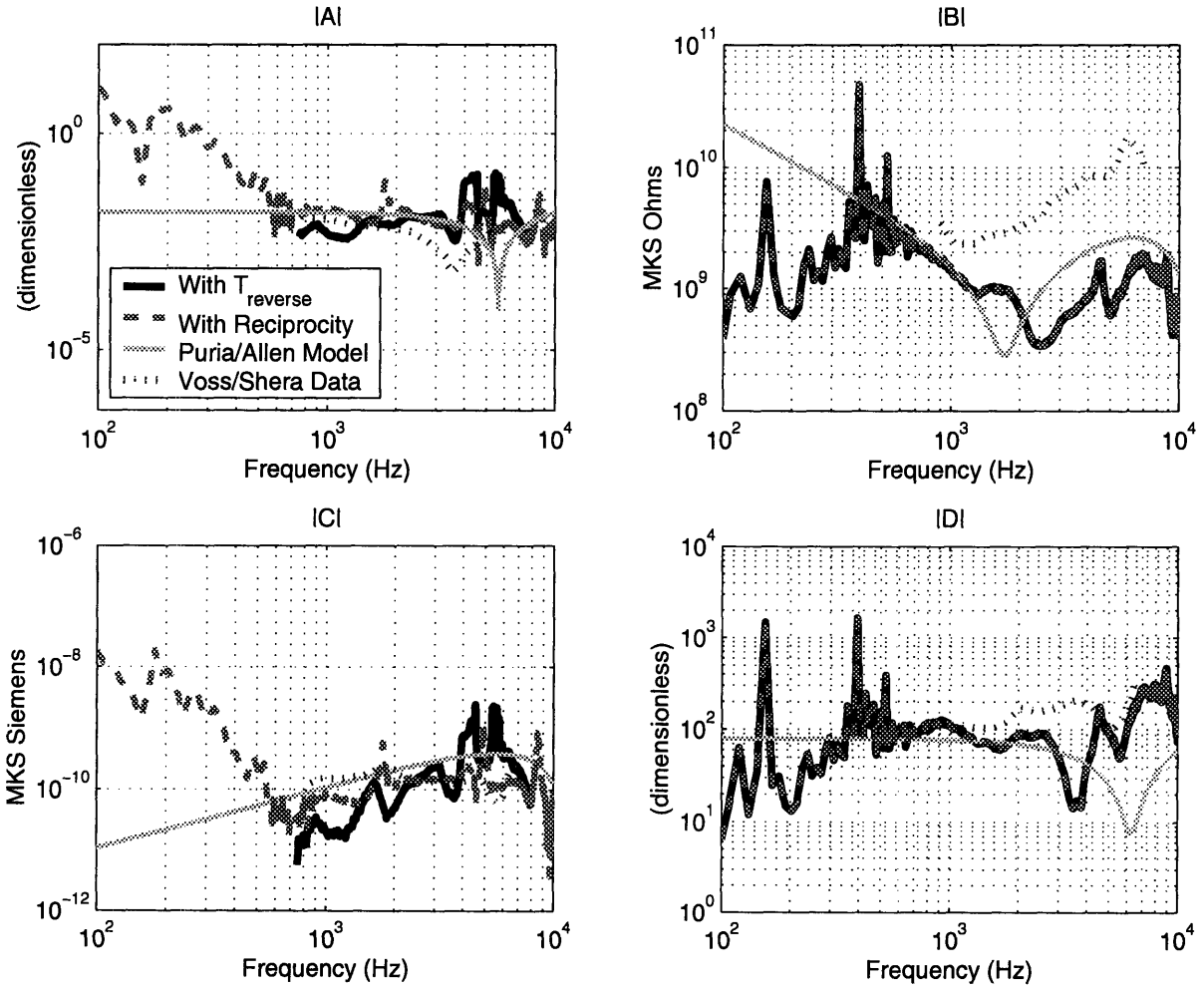

Figure 3-6: Magnitude of the Transmission Matrix Elements.

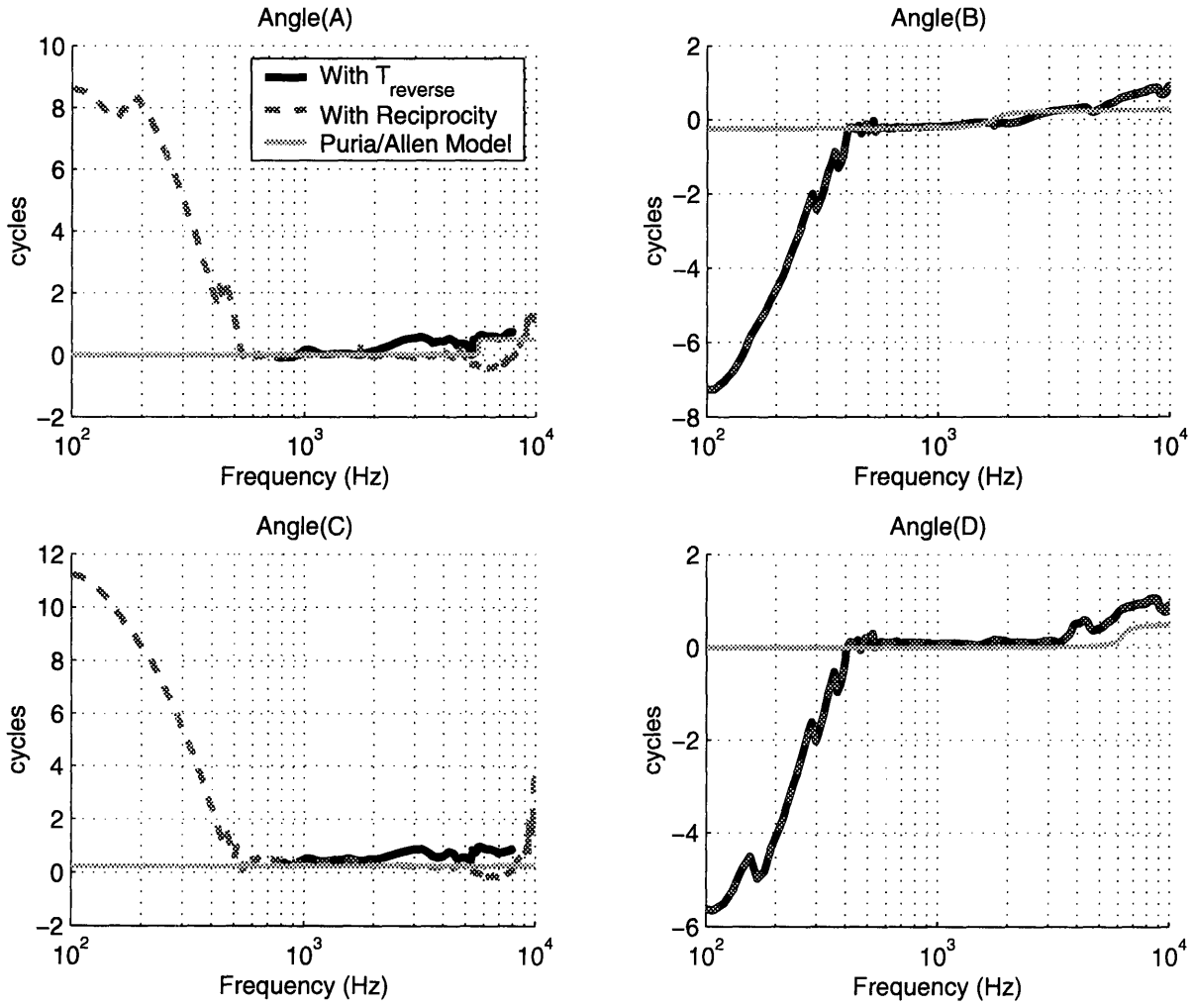

Figure 3-7: Phase of the Transmission Matrix Elements.

Chapter 4

Discussion

4.1 Error Analysis

When trying to decide which equations to use in order to solve for the unknown system parameters, it is useful to look at the potential problems arising from numerical errors in the calculations. From statistics we know that the relative error of an algebraic combination of measurement variables can be calculated using a formula involving the sum of the partial derivatives with respect to all of the uncorrelated measurement variables. For convenience, we will assume that all the measurement variables have a ten percent relative error. Below is the formula 4.1 for the calculation of the relative error where f is the set $[A_{me}, B_{me}, C_{me}, D_{me}]$ and the x_i are all of the measurement variables.

$$\frac{\Delta f}{f} = \frac{\sqrt{\sum_{i=1}^{n} \left(\frac{\partial_i f}{\partial x_i} \Delta x_i\right)^2}}{f} \tag{4.1}$$

In order to use the relative error formula, we will need to input typical measurement values from a middle-ear model created by Puria and Allen [7]. Figure 4-1 shows the topology of the lumped element acoustic circuit. In implementing their model, all of the parameter values from their paper were used. The result for the transmission matrix elements can be seen in Figure 4-2.

Ten percent noise can then be added to each of the simulated measurements made

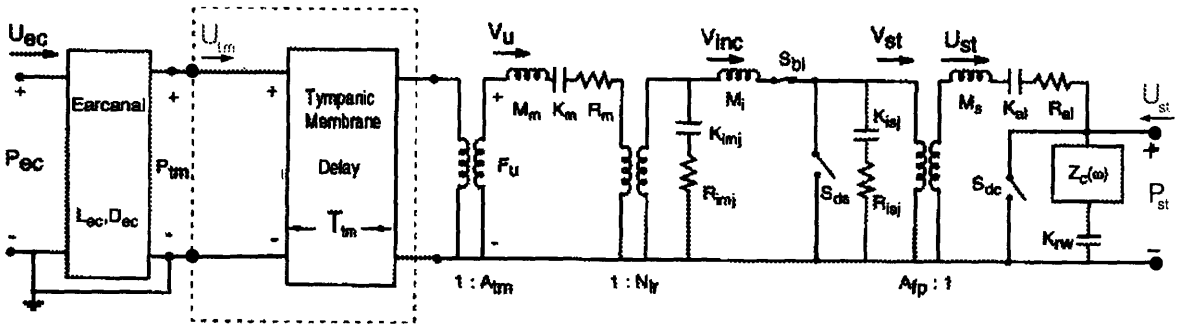

Figure 4-1: Acoustic Lumped Element Middle-ear Model from Puria and Allen [7].

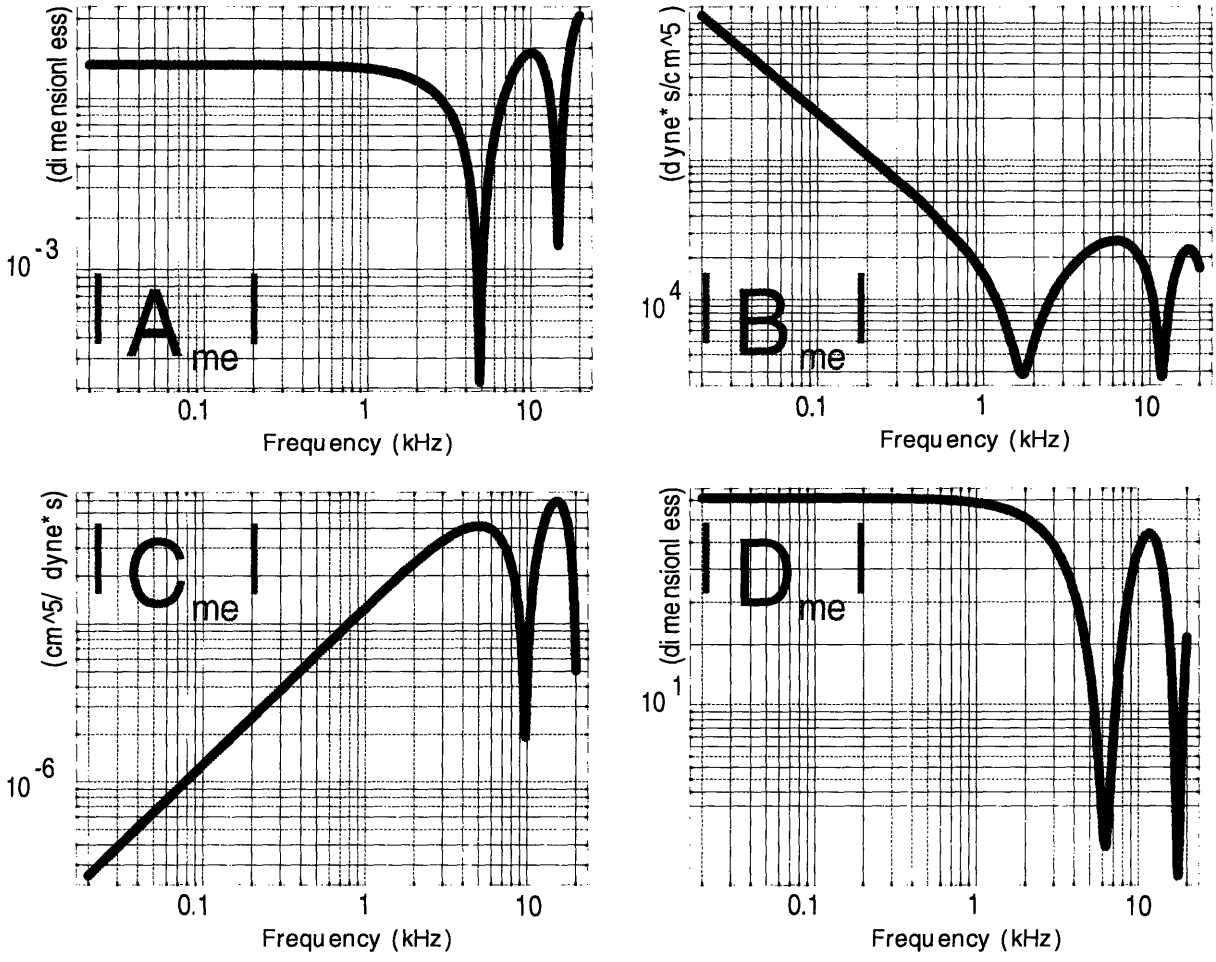

Figure 4-2: Numerical Results for the Transmission Matrix Elements of the Model.

on the model. When these noisy measurements are used to calculate the transmission matrix elements, we find that several of the solutions are inaccurate (see Figure 4-3).

We can understand why certain solutions are inaccurate by calculating the relative

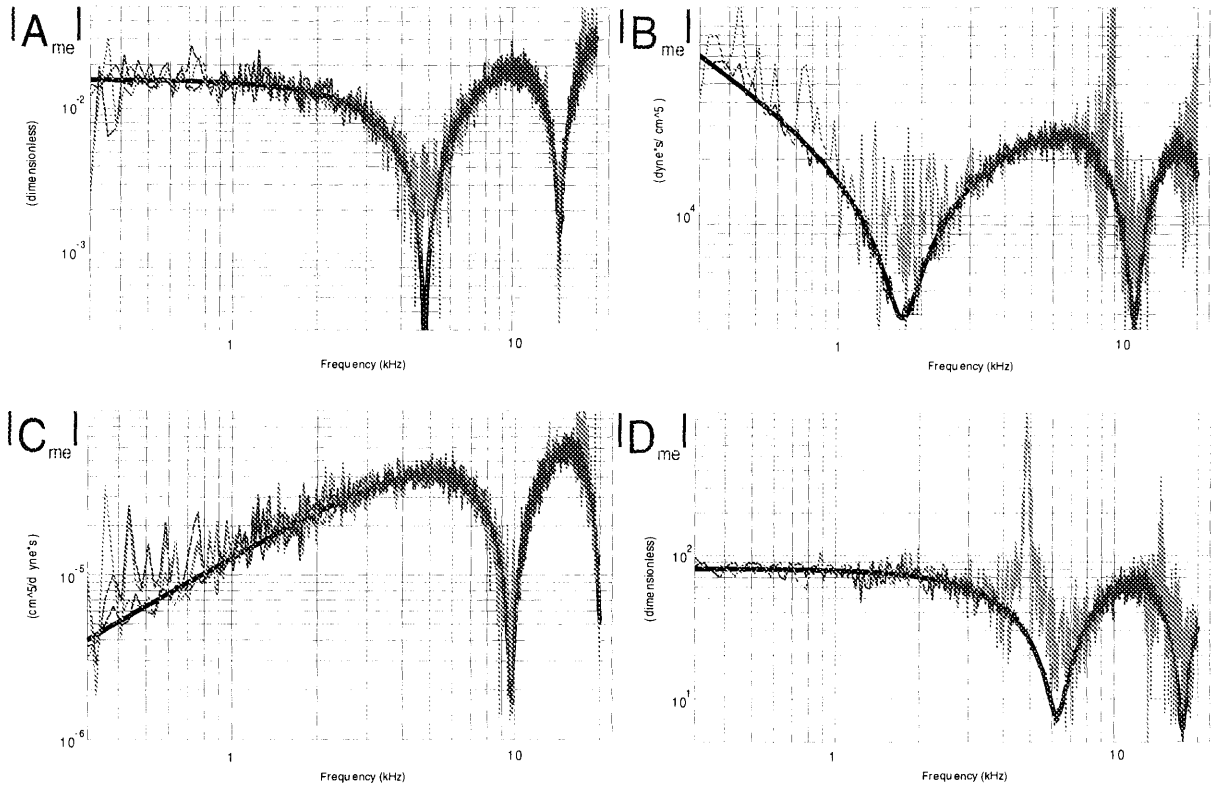

Figure 4-3: Calculation of the Transmission Matrix Elements Using All Solutions.

error for each of the transmission matrix elements (see Figure 4-4). The frequencies where there are large deviations in the calculations for the transmission matrix elements are where the partial derivatives with respect to certian measurement variables are largest.

If we use the relative error curves to eliminate the solutions which are causing problems in the calculations, we can see that the results are relatively impervious to measurement errors in both magnitude and phase (see Figure 4-5).

4.2 Suggested Improvements

The experiment would benefit from a couple of improvements to the technique. First, approximating the 'closed-circuit' condition by fixing the stapes with glue which

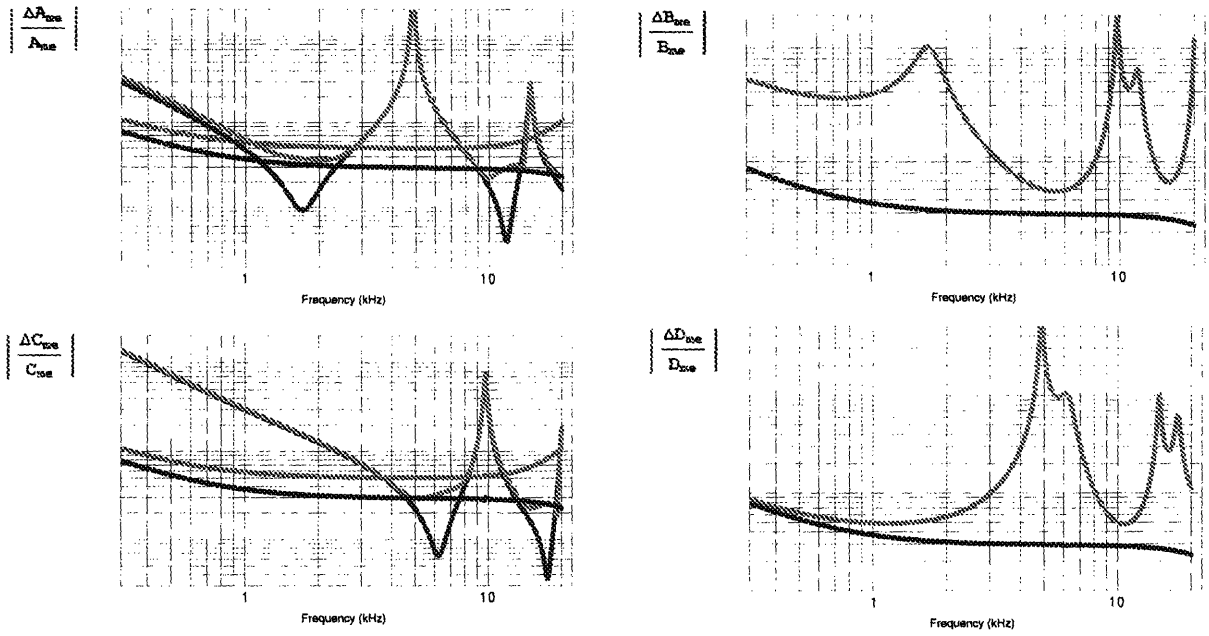

Figure 4-4: Relative Error Curves for the Transmission Matrix Elements.

would allow for an additional equation to be added. This additional equation could be used to further constrain the transmission matrix elements. Additionally, stapes fixation may allow for an experimental confirmation of reciprocity. The choice of experimental animal may need to be reconsidered if the drained cochlea and stapes fixation cases are used to replace the measurement of the reverse transmission using DPOAEs. The cat provides a very stable preparation for long experiments where a lot of data is to be collected from a single animal. An experiment that does not measure the DPOAEs in the stapes velocity is expected to take a fraction of the time, thereby eliminating one of the main reasons for using the cat as an experimental animal. The guinea pig or chinchilla may be a viable alternative to using the cat, with the added benefit of reducing the cost of the experiment.

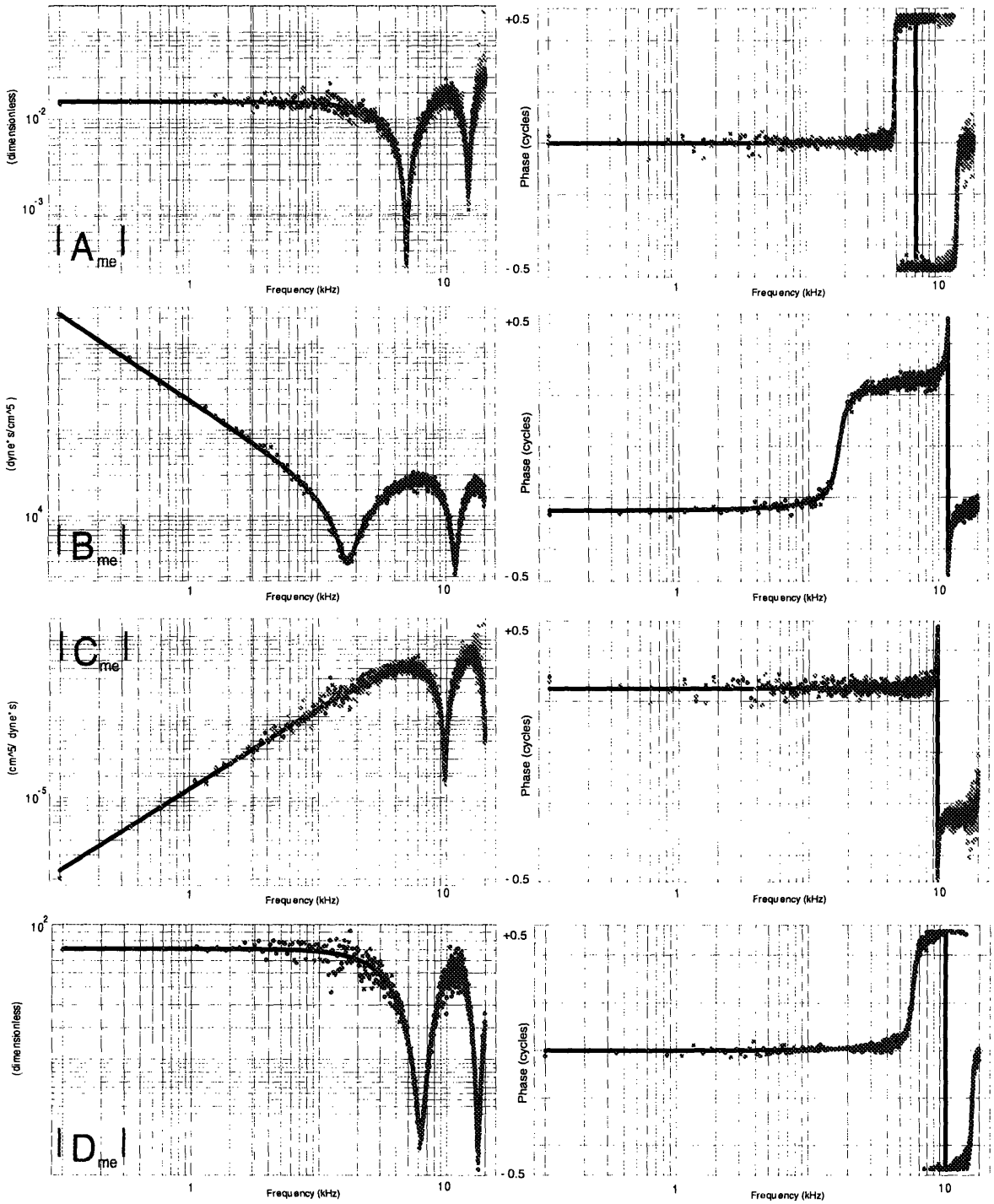

Figure 4-5: Calculation of the Transmission Matrix Elements Using Only the Accurate Solutions.

Bibliography

[1] Allen, J. B. (1986). Measurement of eardrum acoustic impedance. *Peripheral Auditory Mechanisms*, edited by J. B. Allen, J. L. Hall, A. Hubbard, S. T. Neely, and A. Tubis. Springer-Verlag, New York, pp. 44–51.

[2] Avan, P., Buki, B., Maat, B., Dordain, M., and Wit, H. P. (2000). Middle ear influence on otoacoustic emissions. I: Noninvasive investigation of the human transmission apparatus and comparison with model results. *Hearing Research*, **140** 189-201.

[3] Guinan, J. J., and Peake, W. T. (1967). Middle-ear characteristics of anesthetized cats. *J Acoust Soc Am*, **41**(5) 1237–1261.

[4] Keefe, D. H. (1984). Acoustical wave propagation in cylindrical ducts: Transmission line parameter approximations for isothermal and nonisothermal boundary conditions. *J Acoust Soc Am*, **75**(1), 58–62.

[5] Lynch, T. J., Nedzelnitsky, V., and Peake, W.T. (1982). Input impedance of the cochlea in cat. *J Acoust Soc Am*, **72**(1), 108-130.

[6] Lynch, T. J., Peake, W.T., and Rosowski, J. J. (1994). Measurements of the acoustic input impedance of cat ears: 10 Hz to 20 kHz. *J Acoust Soc Am*, **96**(4) 2184-2209.

[7] Puria, S., and Allen, J. B. (1998). Measurements and model of the cat middle ear: evidence of tympanic membrane acoustic delay. *J Acoust Soc Am*, **104**(6) 3463–3481.

[8] Puria, S. (2003). Measurements of human middle ear forward and reverse acoustics: Implications for otoacoustic emissions. *J Acoust Soc Am*, **113**(5) 2773-2789.

[9] Puria, S. (2004). Middle-ear two-port measurements in human cadaveric temporal bones: Comparison with models. *Middle Ear Mechanics in Research and Otology*, edited by A. Gyo and H. Wada. World Scientific, Singapore, pg. 43–50.

[10] Task Force on Newborn and Infant Hearing (1999). Newborn and Infant Hearing Loss: Detection and Intervention. *Pediatrics*, **103** 527–530.

[11] Public Domain Illustration from the National Library of Medicine. NIH Medical Arts & Photography Branch. Published May, 2006. *NIH Publication No. 00-4798.* <http://www.nidcd.nih.gov/health/hearing/coch.asp> Accessed June 29th, 2006.

[12] Shera, C. A., and Zweig, G. (1991). Phenomenological characterization of eardrum transduction. *J. Acoust. Soc. Am.*, **90**(1) 253-262.

[13] Shera, C. A., and Zweig, G. (1992). Middle-ear phenomenology: the view from the three windows. *J Acoust Soc Am*, **92**(3) 1356–1370.

[14] Shera, C.A., and Zweig, G. (1992) An empirical bound on the compressibility of the cochlea. *J. Acoust. Soc. Am.*, **92**(3) 1382-1388.

[15] Shera, C.A., and Guinan, J.J. (1999). Evoked otoacoustic emissions arise by two fundamentally different mechanisms: A taxonomy for mammalian OAEs. *J. Acoust. Soc. Am.*, **105**(2) 782-798.

[16] Voss, S. E., and Allen, J. B. (1994). Measurement of acoustic impedance and reflectance in the human ear canal. *J Acoust Soc Am*, **95**(1) 372–384.

[17] Voss, S. E., Rosowski, J. J., and Peake, W. T. (1996). Is the pressure difference between the oval and round windows the effective acoustic stimulus for the cochlea? *J. Acoust. Soc. Am.*, **100**(3) 1602–1616.

[18] Voss, S. E. (1998). Effects of tympanic-membrane perforations on middle-ear sound transmission: measurements, mechanisms, and models. Ph.D. thesis, Massachusetts Institute of Technology.

[19] Voss, S. E., and Shera, C. A. (2004). Simultaneous measurement of middle-ear input impedance and forward/reverse transmission in cat. *J Acoust Soc Am*, **116**(4 Pt 1) 2187–2198.